Imaging the Cytokine Receptor CXCR4 in Atherosclerotic Plaques with [^{68}Ga]-APD, A Novel Radiotracer on Computer Simulation Approach

Chien-Chung Hsia (hsiacc@yahoo.com)
Institute of Nuclear Energy Research https://orcid.org/0000-0003-2964-1277
Chung-Hsin Yeh
Institute of Nuclear Energy Research
Chun-Tang Chen
Institute of Nuclear Energy Research
Cheng-Liang Peng
Institute of Nuclear Energy Research

Research Article

Keywords: CXCR4, Apo E-/-, Atherosclerosis, APD, Pentixafor

Posted Date: March 2nd, 2022

DOI: https://doi.org/10.21203/rs.3.rs-1331010/v1

Abstract

Background

C-X-C motif chemokine receptor 4 (CXCR4) plays a prominent role in inflammation, atherosclerosis, and cancer biology. Therefore, CXCR4 represents a promising target for molecular imaging in cardiovascular diseases such as atherosclerosis and arterial wall injury. CXCR4 and its cognate ligand, stromal cell–derived factor 1α (SDF-1α), induced monocyte recruitment to the injured endothelium and subsequent plaque formation is the crucial progression of atherosclerosis. CXCR4 was been proved to be intensively expressed on monocytes/macrophage. [^{68}Ga]-APD, based on the structure of CXCR4 antagonists TIQ-15, had designed by computer simulation as a PET tracer for imaging activated macrophages within the atherosclerotic lesions. The aim of this study was to evaluate the biological characteristics of [^{68}Ga]-APD, and compared with the PET tracers targeting atherosclerotic lesion such as [^{18}F]-FDG, [^{18}F]-NaF, and [^{68}Ga]-Pentixafor in apolipoprotein-E-deficient (ApoE$^{-/-}$) mice.

Results

The specification and quality of APD was identified by Mass, NMR and HPLC. After being labeled with Ga-68 under acetate buffer (pH≒5.5), radiochemical purity was over 90% and stable for more than 4 hours in 37°Chuman serum. After being injected from tail vein on ApoE$^{-/-}$ atherosclerotic mice model, hydrophilic [^{68}Ga]-APD was quickly eliminate from the kidney and bladder. [^{68}Ga]-APD could accumulate in the atherosclerotic aorta site and CXCR4 expression organs. The highest target/background ratio (TBR) on atherosclerotic sites were 17.68 ± 0.71 (n = 3) on high-fat diet ApoE$^{-/-}$ mice for 12 weeks after [^{68}Ga]-APD injection within 1 hour. However, [^{68}Ga]-Pentixafor was only 2.06 ± 0.67 (n = 3) on the same mice model. Competitive study represented that CXCR4 antagonist AMD3465 could effectively block the uptake of [^{68}Ga]-APD on the atherosclerotic site and CXCR4 expression organs. Comparing with [^{18}F]-FDG and [^{18}F]-NaF, [^{68}Ga]-APD represented relatively better TBR and specificity on the imaging of atherosclerotic lesions.

Conclusion

In vivo evaluation of CXCR4 expression in ApoE$^{-/-}$ mice revealed the uptake of [^{68}Ga]-APD mainly accumulated in the atherosclerotic aorta site. Moreover, the TBR of [^{68}Ga]-APD was 8 times higher than [^{68}Ga]-Pentixafor, a radiotracer targeting CXCR4 and under phase II clinical trial, indicating this novel tracer [^{68}Ga]-APD is more feasible as a surrogate marker for inflammatory atherosclerosis.

Background

Although the diet management and medical improvement in treating cardiovascular diseases (CVD), atherosclerotic plaque-induced stroke and coronary heart disease (CHD), heart attack, or angina are one of the leading causes of mortality and morbidity worldwide. (1, 2). The pathogenesis of atherosclerosis is characterized by the chronic accumulation of lipids and pro-inflammatory immune cells to the focal arterial wall and progressively narrows the lumen of the artery (3–5). Owing to the unstable plaques by the pathologic mechanisms of inflammation, atherosclerotic plaque formation can be diagnosis from the mechanism of inflammation (6, 7). Within the inflammation and different aspects of the atherosclerotic plaque, activated macrophages play the most interesting target in the atherosclerotic lesion (8).

Imaging atherosclerosis with PET/CT characterizes atherosclerotic plaques on a molecular level and enables the quantification of arterial calcification (9). Many Functional PET imaging tracers have been tried to targeting molecular elements of atherosclerosis of increasing the glucose metabolism by the inflammatory cells (10–13) and detect micro-calcifications around the arterial wall (14–16), such as [^{18}F]-FDG and [^{18}F]-NaF, respectively.

The 7-transmembrane helix G-protein–coupled receptor, Chemokine C-X-C motif receptor 4 (CXCR4), and its cognate ligand, stromal cell–derived factor 1a (SDF-1a/CXCL12), induced monocyte recruitment to the injured endothelium and subsequent plaque formation is the crucial progression of atherosclerosis. CXCR4 is also been proven to be intensively expressed on monocytes/macrophage (17–21). Recently, CXCR4-directed of macrophages PET imaging with [^{68}Ga]-radiolabeled cyclic peptide, Pentixafor, has been provided to imaging neoplasms, hematologic, stroke, atherosclerosis, and myocardial infarction in humans by the mechanism of overexpression CXCR4 (22–25). In addition, Tetra-azamacrocycles based small-molecule CXCR4 antagonists, such as AMD3100 and AMD3465, are also developed and proven to bind on human and mouse variants CXCR4 receptor. Orit Jacobson et al. had developed a one step radiosynthesis of [^{64}Cu]- AMD3100 and exhibited a promising agent for visualization of CXCR4-positive tumors and metastases (26). However, Copper(II) cyclam complexes are unlikely to have sufficient electrostatic/H-bonding between cyclam amine groups with aspartate residue side chains (171 and 262) and lead to high nonspecific hepatic accumulation to retain the metal ion *in vivo* (27).

The atherosclerotic-prone apolipoprotein E-deficient (ApoE$^{-/-}$) mice were first developed in 1992 by homologous recombination of embryonic stem cells and currently use in the pre-clinical atherosclerotic model by downregulation of cholesterol transporter ATP-binding cassette subfamily A member 1 levels (28). Poor lipoprotein clearance of atherosclerosis-prone apolipoprotein E-deficient (Apoe$^{-/-}$) mice display the accumulation of cholesterol ester-enriched particles in the blood and promote the development of atherosclerotic plaques. ApoE$^{-/-}$ mice is well established for studying atherosclerotic lesions by high-fat chow diet or even a regular diet for several weeks. The atherosclerotic lesions in ApoE$^{-/-}$ mice resemble human lesions in their predilection sites and progression to the fibro-proliferative stage (29).

In this study, we investigate the biological characteristics of novel CXCR4 agent [^{68}Ga]-APD, and compared with other PET tracers targeting atherosclerotic lesion such as [^{18}F]-FDG, [^{18}F]-NaF, and [^{68}Ga]-

Pentixafor in the ApoE$^{-/-}$mice model with high fat diet.

Materials And Methods

General

Computer simulation BIOVIA Discovery Studio designed APD from Tetrahydroisoquinoline-Based CXCR4 Antagonist TIQ-15 (Fig.1) by screening million's chemical fragments with chemical binding energy and CDOCKER on CXCR4 specific amino acids residue by H-bond, pi-pi interaction (30). APD synthesized at RDD LAB. INC, Taiwan and determined its specifications by NMR (JNM-ECZ500R/S1, JOEL USA, Inc), Mass (AB Sciex (Concord, ON, Canada) 4000QTRAP® mass spectrometry) and high-performance liquid chromatography (HPLC, Waters-2695, with UV and radio detector). Radio-thin-layer chromatography was performed on instant TLC chromatogram sheets (Sigma Chemical Company, USA), eluting with citrate buffer (pH=5.5) and Bioscan AR-2000 (Eckert & Ziegler, Germany). Pentixafor purchased from UNION CHEMICAL IND. CO., LTD. Taiwan. [^{18}F]-FDG and [^{18}F]-NaF provided from Institute of Nuclear Energy Research, Taoyuan, Taiwan.

Preparation and radiochemical purity (RCP) analysis

APD (0.01~0.1mg) dissolved in acetate buffer (pH 5.0~6.0) and then labeled with [^{68}Ga]-$GaCl_3$ (1~10mCi) for at least 20 minutes under 60~70℃.To determine the amount of impurity free Ga-68, the sample was chromatographed on ITLC-SG (Sigma Chemical Company, USA) using 0.1 M citrate buffer (pH 5.5) as the mobile phase. Free Ga-68 migrated with the solvent front, whereas labeled [^{68}Ga]-APD remained at the origin. A Waters system pump (Germering, D) and radiometric detection (Bioscan, Washington DC), were used for RP-HPLC analysis. C-18 column (Waters 5 μm, 80 Å, 250 × 4.6 mm). Flow rates of 0.8 mL/min were employed as the following: a linear gradient eluent starting from 30% A (0.1% TFA in water) and 70% B (0.1% TFA in acetonitrile), increasing to 90% B for 10 min, remaining constant at 90% B for another 15–30 min. The RCP was calculated expressing the peak corresponding to [^{68}Ga]-APD as percentage of the total activity in the radio-chromatogram. The injected activity on the HPLC-column was in the order of 5 MBq. RCP of [^{68}Ga]-Pentixafor was also determined by HPLC followed as previously described (31).

Partition Coefficient (n-Octanol/PBS) Determination

To determine the hydrophilicity of [^{68}Ga]-APD, the octanol/water partition coefficients (log P) were measured. Briefly, [^{68}Ga]-APD (7.4 MBq) with phosphate-buffered saline (PBS, 5.0 mL, 0.15 M, pH 7.4) and n-octanol (5 mL) within a test tube. After vortexing for 1 min, tube was placed on bench for 3 min in room temperature. Samples (from each phase, 100 μL) were counted its radioactivity by using gamma-counter. The tests were reported as mean ± SD (n≧3), independently.

Mice and PET/CT Acquisition

ApoE$^{-/-}$ mice experimental protocol had been approved by the Institutional Animal Care and Use Committee (IACUC) in the Institute of Nuclear Energy Research (Taoyuan, Taiwan) and followed the ARRIVE guidelines and the USPHS Policy on Human Care and Use of Laboratory Animals. Female ApoE$^{-/-}$ mice (provided from Taiwan University Hospital) (aged >8 weeks) housed in a controlled environment (22 ± 2°C and 50 ± 5% relative humidity) with a 12-h light-and-dark cycle and received a high-fat diet for accelerating atherosclerotic sites. PET/CT imaging was performed on a Bioscan scanner (matrix size, 128 × 128 × 159; CT attenuation-corrected; non-scatter corrected) (Washington DC, USA) following a intravenous tail vein injection of approximately 14.8 MBq (0.4 mCi) of [^{68}Ga]-APD into ApoE$^{-/-}$ mice (3–5 mice per group). Dynamic scans were acquired in list mode format for at least 120 min, and sorted into 22 frames, 0.5-mm sinogram bins for image reconstruction (4 × 15 s, 4 × 60 s, 11 × 300 s, 3 × 600 s). Mice were anesthetized with isoflurane (3% for induction and 2% for maintenance) throughout the experiment.

ApoE$^{-/-}$ mice was imaged with [^{68}Ga]-APD (11.1 MBq) on 2, 8 and 12 weeks of high-fat diet to characterize atherosclerotic lesions. For competitive inhibition assay on [^{68}Ga]-APD, a CXCR4 inhibitor AMD3465 (25 mg/kg) was injected before administration of 11.1 MBq of [^{68}Ga]-APD on high-fat diet ApoE$^{-/-}$ mice for 12 weeks. [^{68}Ga]-Pentixafor (11.1 MBq) was also administrated on the same mice model for comparing the efficacy on atherosclerotic lesions with [^{68}Ga]-APD. [^{18}F]-FDG PET/CT imaging was been performed after 6 h fasting period to ensure serum glucose levels below 130 mg/dL. To estimate the radioactivity concentration, volumes of interests had defined on coregistered PET/CT images using PMOD software. Target/Background Ratio (TBR) had calculated by placing a circular 2-mm volume of all interest organs/tissues around a site. TBRs were been calculated as focal uptake divided by blood pool.

Autoradiographic studies on atherosclerosis

To visualize the distribution of [^{68}Ga]-APD in the heart and aorta, autoradiography was performed using 20-μm-thick fresh-frozen heart and aorta sections derived from ApoE$^{-/-}$ mice. The specimens were exposed to phosphor imaging plates (MS-2040, Fuji Photo Film Co. Ltd.) for 2 h in the [^{68}Ga]-APD examination. Subsequently, the radioactivity distributions were imaged by using imaging analyzer BAS 4000 (Fuji Photo Film Co. Ltd.).

Statistical analysis

The statistical significance of comparisons of radioactivity in organs in PET studies was based on 2-sided, 2-sample Student t-tests. For all tests, $P < 0.05$ was considered statistically significance and represented on figures. Results were reported as mean ± SD ($n \geqq 3$).

Results

Synthesis and Characterization

The novel CXCR4 antagonist structure of APD was represented. (Fig.1) The binding energy and CDOCKER energy of APD were -300.33 kcal/mol and -57.01kJ/mol, respectively. However, the binding energy of TIQ-15 was only -88 kcal/mol. After the synthesis, chemical characterization had verified by NMR, mass spectrum and HPLC. ^{1}H NMR (D_2O) d 8.46-8.45 (m, 1 H), 7.84-7.80 (m, 2.H), 7.49-7.47 (d, 1H), 7.41-7.34(m, 3H), 3.70-3.90 (m,6H), 2.78-2.47 (m, 20H), 1.73-1.67 (m, 2H). ^{13}C NMR (D_2O) d160.30, 157.53, 148.16, 138.61, 137.96, 124.63, 123.08, 122.84, 120.45, 59.98, 53.29, 50.30, 45.93, 45.10, 43.92, 43.29, 23.31. The molecular weight and purity of APD was measured as $[M+H]^+$=441.51 and over 98%, respectively.

Radiochemical purity (RCP) and Partition Coefficient (n-Octanol/PBS) Determination

APD (0.01~0.1mg) dissolved in acetate buffer (pH 5.0~6.0) and then labeled with [^{68}Ga]-$GaCl_3$ (1~10mCi) for at least 20 mins under 60~70℃.Radiochemical purity of [^{68}Ga]-APD was calculated by paper chromatography on SG-ITLC strip with citrate buffer (pH5.5) (Fig. 2A). Free Ga-68 would migrate to solvent front, whereas [^{68}Ga]-APD remained nearly at the origin. The chromatogram represented that the radiochemical purity of [^{68}Ga]-APD was over 90%. In addition, according to the Radio-HPLC chromatogram (Fig. 2B), the retention time of [^{68}Ga]-APD and impurity-free Ga-68 was represented at about 13.2 min and 3.5 min, respectively. The radiochemical purity of [^{68}Ga]-APD was also verified over 90% by HPLC analysis. Furthermore, [^{68}Ga]-APD was stable under room temperature and even in 37℃human serum for over 4 hours. Its primary decomposition of radio-product appeared to be free Ga-68. The partition coefficient of [^{68}Ga]-APD was determined as 0.040±0.0029 (n=4) which was shown its good hydrophilicity.

PET/CT Studies on ApoE$^{-/-}$ atherosclerotic model mice

In the competitive inhibition study, the PET/CT images represented that [^{68}Ga]-APD could be apparently blocked the uptake on atherosclerotic lesion by pre-injection of a dose (5 mg/kg) of CXCR4 inhibitor AMD3465 on high fat diet ApoE$^{-/-}$ mice for 12weeks. Furthermore, the pre-dosing with AMD-3465 could also significantly reduce the TBR of [^{68}Ga]-APD at CXCR4-overexpression organs, such as liver, lung, and kidney (27). These evidences provided that [^{68}Ga]-APD was specific binding on CXCR4 ($P<0.05$). (Fig.3)

In comparing the PET images of [^{68}Ga]-APD (11.1 MBq) on the different duration ApoE$^{-/-}$ mice, the TBR was 7.52 ± 0.83, 9.65 ± 0.69 and 17.68 ± 0.71 on 2, 8 and 12 weeks of high fat diet, respectively. The TBR of [^{68}Ga]-APD was decreased with time (n=3) (Fig.4). Kidney and bladder had higher tracer uptake, providing that [^{68}Ga]-APD might primarily excrete from the kidney to bladder.

For comparing the imaging efficacy on atherosclerotic lesions between [^{68}Ga]-APD and [^{68}Ga]-Pentixafor (RCP>95%), tracers (11.1 MBq) were injected on high-fat diet ApoE$^{-/-}$ mice for 12 weeks. The TBR result represented that [^{68}Ga]-APD had about 8 times higher than [^{68}Ga]-Pentixafor during the imaging

time (Fig.5). The results of TBR on [^{68}Ga]-Pentixafor was almost matched as previously described (22-25).

[^{18}F]-FDG injection was been performed after fasting for at least 6 h to ensure serum glucose levels below 130 mg/dL. The PET image represents that [^{18}F]-FDG accumulated mainly on the myocardium. However, the highest TBR of [^{18}F]-FDG was only 1.53±0.75 (n=3) on the atherosclerotic lesions on high-fat diet ApoE$^{-/-}$ mice for 10 weeks. Furthermore, [^{18}F]-NaF could not effectively target atherosclerotic site by the reason of lacking calcified lesions on only 10 weeks of high-fat diet. (Fig.6)

Autoradiographic studies on atherosclerosis

From the PET/CT image of [^{68}Ga]-APD (Fig 6), there was tracer specific targeting in the chest region. For verified the distribution of [^{68}Ga]-APD, the slide autoradiogram of [^{68}Ga]-APD (Fig.7) had shown obvious high radioactivity accumulating in the aorta region but not on the heart.

Discussion

This study reports a novel CXCR4 antagonist structure APD was been designed by replacing over million's chemical fragments on the structure of TIQ-15 and evaluating its docking efficacy by computer simulation approach. After being labeled with Ga-68, [^{68}Ga]-APD represent good sensitivity and specificity to CXCR4 expression atherosclerotic lesions.

Atherosclerotic plaque formation, development, and progression are complex and involve many factors, including endothelial dysfunction, elevated cholesterol and immune activity. As plaques in the arterial walls build and progress, the rupture on the arteries may be occluded distally and block blood flow into heart muscle, brain, and other parts of the body (1). Inflammation is an important component of atherosclerotic plaque vulnerability. Owing to the glucose uptake in active and lipid-rich macrophages on inflammatory plaques, it is likely to use [^{18}F]-FDG as a marker to detect small lesions of atherosclerotic plaques. However, [^{18}F]-FDG plaque imaging is limited by non-specificity on atherosclerotic lesions. In addition, the constant motion of cardiac cycle and the significant uptake of [^{18}F]-FDG in the myocardium has decreased the enthusiasm to use this tracer in atherosclerotic imaging (25). [^{18}F]-NaF have significant advantages in the assessment of atherosclerotic plaques imaging with regards to its more accurately and precisely in detecting and characterizing plaques than [^{18}F]-FDG. Therefore, the future of PET imaging to assess atherosclerosis will predict to heavily rely on [^{18}F]-NaF (32).

Oxidized low-density lipoprotein (Ox-LDL) and vascular hypoxic process might significantly induce macrophage to overexpression CXCR4 and enhanced the atherosclerotic progression. In comparison within early or advanced atherosclerotic lesions, Ilze Bot et al. had found that CXCR4 expression was significantly pronounced in advanced unstable lesions (33). Remarkably, the expression of CXCR4 protein was co-localized with macrophage expression in inflamed vulnerable plaque lesions. This finding might

support the concept that CXCR4 played a recruitment role for leukocytes into the vessel wall and could serve as a good biomarker for atherosclerotic imaging (27).

There are many PET tracers have tried to image atherosclerotic changes based on the macrophage to expression CXCR4. [^{68}Ga]-Pentixafor is one of the successful CXCR4 clinical trial tracers to image atherosclerosis with a clear view of vascular uptake and a relatively clear background. Xiang Li et al. had shown that patients with higher uptake of [^{68}Ga]-Pentixafor represented a higher incidence of metabolic syndrome and might suggest its clinical potential in the evaluation of diseased vessels (34). Derlin T. et al. had also shown that accumulation of [^{68}Ga]-Pentixafor and [^{18}F]-FDG represented only a weak correlation by observed in non-calcified lesions (35).

Tetrahydroisoquinoline-Based CXCR4 antagonists TIQ-15 had been found to have good oral bioavailability and its active structure was confirmed to interaction with ASP 97, Tyr116 and Glu288 residue on CXCR4 (36). In this study, a novel CXCR4 tracer APD was been designed from the structure of TIQ-15 by computer simulation approach. The selected structure of APD was been screened by replacing over million's chemical fragments on the structure of TIQ-15 and evaluating its docking efficacy. The simulating binding energy of APD and TIQ-15 was − 300.33 and − 88kcal/mol, respectively. In our preliminary study, [^{68}Ga]-APD had showed specific binding on CXCR4-expression MDA-MB231 breast cancer cells and could be blocked the cellular uptake by using CXCR4 antagonist AMD3465. The PET image of [^{68}Ga]-APD on ApoE$^{-/-}$ atherosclerotic model had shown high selective uptake on atherosclerotic lesions. Owing to its high hydrophilicity (Partition coefficient = 0.040 ± 0.0029), [^{68}Ga]-APD PET image showed a quick excretion from kidney and with a relatively low background. CXCR4 antagonist AMD465 (5 mg/kg) could effectively reduce the uptake on atherosclerotic plaque, liver, lung and kidney at 60 min before tracer administration which suggested its specific binding on CXCR4 (Fig. 3). Further experiments demonstrated that more than 90% of urine radioactivity was intact [^{68}Ga]-APD. Human serum stability assays also showed that [^{68}Ga]-APD could be stable for over 4 h under 37℃ human serum. For confirming the distribution of isotope labeled APD on the atherosclerotic sites, tissue frozen section had also been done after the bio-distributed of [^{68}Ga]-APD (RCP > 90%) for 30 mins on ApoE$^{-/-}$ mice. The autoradiogram represented that [^{68}Ga]-APD was major distributed on aorta, but not in the heart (Fig. 7).

Atherosclerotic plaques may stabilize or reduce in size, lipid content, foam cell content, and macrophage inflammation through Macrophage Reverse Cholesterol Transport (RCT) mechanism by eliminating oxidized low-density lipoprotein (Ox-LDL) from atherosclerotic plaques. (37, 38). Early detection and therapy is the key to improving the atherosclerotic prognosis at present. In this study, [^{68}Ga]-APD PET image provides the possibility in the early diagnosis of atherosclerosis with high sensitivity and specificity than [^{68}Ga]-Pentixafor by targeting CXCR4-overexpression macrophage.

Conclusion

In vivo evaluation of CXCR4 expression in ApoE$^{-/-}$ mice revealed the uptake of [^{68}Ga]-APD mainly accumulated in the atherosclerotic aorta site. Moreover, the TBR of [^{68}Ga]-APD was 8 times higher than [^{68}Ga]-Pentixafor, a radiotracer targeting CXCR4 and under phase II clinical trial, indicating this novel tracer [^{68}Ga]-APD is more feasible as a surrogate marker for inflammatory atherosclerosis.

List Of Abbreviations

CXCR4: C-X-C motif chemokine receptor 4; SDF-1a: stromal cell–derived factor 1a; APD: 6-Aminomethyl-pyridin-2-ylmethyl)-pyridin-2-ylmethyl-[3-(1,4,7,10tetraaza-cyclododec-1-yl)-propyl]-amine; ApoE$^{-/-}$: apolipoprotein-E-deficient; TBR: target/background ratio; RCP: radiochemical purity.

Declarations

Ethics approval and consent to participate

ApoE$^{-/-}$ mice experimental protocol had approved by the Institutional Animal Care and Use Committee (IACUC) in the Institute of Nuclear Energy Research (Taoyuan, Taiwan) and followed the ARRIVE guidelines and the USPHS Policy on Human Care and Use of Laboratory Animals. ApoE$^{-/-}$ mice had gotten the consent to provide from Taiwan University Hospital.

Consent for publication

Not applicable

Availability of data and material

All the raw data of this study, including PET images, can be obtained through the corresponding authors on reasonable request.

Competing interests

The authors declare that no other potential conflict of interest relevant to this article exist.

Funding

Funding was all provided by Institute of Nuclear Energy Research, Taiwan.

Authors' contributions

CH conducted experiments and wrote the manuscript. CY, CC and CP reviewed the study design and helped to cultured cells, raised mice and conducted mice's experiments. All authors read and approved the final manuscript.

Acknowledgements

I would like to express my deep and sincere gratitude to research colleagues, Dr. Mei-Hui Wang, Dr. Hung-Wen Yu, Dr. Ying-Hsia Shih and all of the teams' member for his genuine support throughout this research work. I thank the management of Institute of Nuclear Energy Research for their financial support to do this work. I also thank the directors Dr. Shiou-Shiow Farn, Dr. Jeng-Hung Lee and Dr. Jeng-Jong Wang and Dr. Chih-Hsien Chang for their genuine support to complete this thesis successfully. Finally, my thanks go to all the people who have supported me to complete the research work directly or indirectly.

References

1. Eric Munger, John W. Hickey, Amit K. Dey, Mohsin Saleet Jafri, Jason M. Kinser, and Nehal N. Mehta. Application of machine learning in understanding atherosclerosis: Emerging insights. APL Bioeng. 2021; 5(1): 011505. https://doi.org/10.1063/5.0028986
2. Takehiro Nakahara & H. William Strauss. From inflammation to calcification in atherosclerosis. Eur J Nucl Med Mol Imaging. 2017; 44:858–860. https://doi.org/10.1007/s00259-016-3608-x
3. D. E. Bild, D. A. Bluemke, G. L. Burke et al., "Multi-ethnic study of atherosclerosis: Objectives and design," Am. J. Epidemiol. 2002; 156(9): 871–881. https://doi.org/10.1093/aje/kwf113
4. C. J. Cooper, T. P. Murphy, D. E. Cutlip et al., "Stenting and medical therapy for atherosclerotic renal-artery stenosis," N. Engl. J. Med. 2014; 370(1): 13–22. https://doi.org/10.1056/NEJMoa131075
5. T. Chen, P. Brewster, K. R. Tuttle et al., "Prediction of cardiovascular outcomes with machine learning techniques: Application to the cardiovascular outcomes in renal atherosclerotic lesions (CORAL) study," Int. J. Nephrol. Renovasc. Dis. 2019;12: 49–58. https://www.ncbi.nlm.nih.gov/pmc/articles/PMC6433104/pdf/ijnrd-12-049.pdf
6. Peter Libby. History of Discovery: Inflammation in Atherosclerosis. Arterioscler Thromb Vasc Biol. 2012;32(9): 2045–2051. https://doi.org/10.1161/ATVBAHA.108.179705.
7. Silvestre-Roig C, Winther MPd, Weber C, Daemen MJ, Lutgens E, Soehnlein O. Atherosclerotic Plaque Destabilization. Circ Res. 2014; 114(1):214–226. https://doi.org/10.1161/CIRCRESAHA.114.302355
8. Moore KJ, Sheedy FJ, Fisher EA. Macrophages in atherosclerosis: a dynamic balance. Nat Rev Immunol. 2013;13(10):709-721. https://doi.org/10.1038/nri3520
9. Joseph P, Tawakol A. Imaging atherosclerosis with positron emission tomography. Eur Heart J. 2016; 37(39):2974–2980. https://doi.org/10.1093/eurheartj/ehw147
10. Tarkin JM, Joshi FR, Evans NR, Chowdhury MM, Figg NL, Shah AV, et al. Detection of Atherosclerotic Inflammation by ^{68}Ga-DOTATATE PET Compared to [^{18}F]FDG PET Imaging. J Am Coll Cardiol. 2017; 69(14):1774–1791. https://doi.org/10.1016/j.jacc.2017.01.060
11. Pauwels EKJ, Sturm EJC, Bombardieri E, Cleton FJ, Stokkel MPM. Positron-emission tomography with [^{18}F]fluorodeoxyglucose. J Cancer Res Clin Oncol. 2000; 126(10):549–559. https://doi.org/10.1007/s004320050028
12. Hetterich H, Rominger A,Walter L, et al. Natural history of atherosclerotic disease progression as assessed by (^{18})F-FDG PET/CT. Int J Cardiovasc Imaging. 2016; 32:49–

59. https://doi.org/10.1007/s10554-015-0660-8

13. Rudd JH,Myers KS, Bansilal S, et al. Atherosclerosis inflammation imaging with ^{18}F-FDG PET: carotid, iliac, and femoral uptake reproducibility, quantification methods, and recommendations. J Nucl Med: Off Publ SocNucl Med. 2008; 49:871–878. https://doi.org/10.2967/jnumed.107.050294
14. Derlin T, Richter U, Bannas P, et al. Feasibility of ^{18}F-sodium fluoride PET/CT for imaging of atherosclerotic plaque. J Nucl Med: Off Publ SocNucl Med. 2010; 51:862–865. https://doi.org/10.2967/jnumed.110.076471
15. Derlin T, Wisotzki C, Richter U, et al. In vivo imaging of mineral deposition in carotid plaque using ^{18}F-sodium fluoride PET/CT: correlation with atherogenic risk factors. J Nucl Med: Off Publ SocNucl Med. 2011; 52:362–368. https://doi.org/10.2967/jnumed.110.081208
16. Fiz F, Morbelli S, Piccardo A, et al. ^{18}F-NaF uptake by atherosclerotic plaque on PET/CT imaging: inverse correlation between calcification density and mineral metabolic activity. J Nucl Med: Off Publ SocNucl Med. 2015; 56:1019–1023. https://doi.org/10.2967/jnumed.115.154229
17. Zernecke A, Bot I, Djalali-Talab Y, Shagdarsuren E, Bidzhekov K, Meiler S, et al. Protective Role of CXC Receptor 4/CXC Ligand 12 Unveils the Importance of Neutrophils in Atherosclerosis. Circ Res. 2008; 102(2):209–217. https://doi.org/10.1161/CIRCRESAHA.107.160697
18. Döring Y, Noels H, Vorst EPCvd, Neideck C, Egea V, Drechsler M, et al. Vascular CXCR4 Limits Atherosclerosis by Maintaining Arterial Integrity. Circulation. 2017;136(4):388–403. https://doi.org/10.1161/CIRCULATIONAHA.117.027646
19. Döring Y, Vorst EPCvd, Duchene J, Jansen Y, Gencer S, Bidzhekov K, et al. CXCL12 Derived From Endothelial Cells Promotes Atherosclerosis to Drive Coronary Artery Disease. Circulation. 2019; 139(10):1338–1340. https://doi.org/10.1161/CIRCULATIONAHA.118.037953
20. Merckelbach S, van der Vorst EPC, Kallmayer M, Rischpler C, Burgkart R, Döring Y, et al. Expression and Cellular Localization of CXCR4 and CXCL12 in Human Carotid Atherosclerotic Plaques. Thromb Haemost. 2018; 118(01):195–206. https://doi.org/10.1160/TH17-04-0271
21. Demmer O, Gourni E, Schumacher U, Kessler H, Wester H-J. PET Imaging of CXCR4 Receptors in Cancer by a New Optimized Ligand. ChemMedChem. 2011; 6(10):1789–1791. https://doi.org/10.1002/cmdc.201100320
22. Hyafil F, Pelisek J, Laitinen I, Schottelius M, Mohring M, Döring Y, et al. Imaging the Cytokine Receptor CXCR4 in Atherosclerotic Plaques with the Radiotracer ^{68}Ga-Pentixafor for PET. J Nucl Med. 2017; 58(3):499–506. https://doi.org/10.2967/jnumed.116.179663
23. Weiberg D, Thackeray JT, Daum G, Sohns JM, Kropf S, Wester H-J, et al. Clinical Molecular Imaging of Chemokine Receptor CXCR4 Expression in Atherosclerotic Plaque Using ^{68}Ga-Pentixafor PET: Correlation with Cardiovascular Risk Factors and Calcified Plaque Burden. J Nucl Med. 2018; 59(2):266–272. https://doi.org/10.2967/jnumed.117.196485
24. Derlin T, Sedding DG, Dutzmann J, Haghikia A, Konig T, Napp LC, et al. Imaging of chemokine receptor CXCR4 expression in culprit and nonculprit coronary atherosclerotic plaque using motion-

corrected [(^{68})Ga]pentixafor PET/CT. European journal of nuclear medicine and molecular imaging. 2018; 45(11):1934–1944. https://doi.org/10.1007/s00259-018-4076-2

25. Constantin Lapa1, Martin Schreder, Andreas Schirbel, Samuel Samnick, Klaus Martin Kortüm, Ken Herrmann, Saskia Kropf, Herrmann Einsele, Andreas K. Buck, Hans-Jürgen Wester, Stefan Knop, Katharina Lückerath. [68Ga]Pentixafor-PET/CT for imaging of chemokine receptor CXCR4 expression in multiple myeloma - Comparison to [18F]FDG and laboratory values. Theranostics 2017; 7(1):205-212. https://doi.org/10.7150/thno.16576
26. Orit Jacobson, Ido D. Weiss, Lawrence Szajek, Joshua M. Farber, Dale O. Kiesewetter. ^{64}Cu-AMD3100—A novel imaging agent for targeting chemokine receptor CXCR4. Bioorganic & Medicinal Chemistry. 2009; 17:1486–1493. https://doi.org/10.1016/j.bmc.2009.01.014
27. Benjamin P. Burke, Cecilia S. Miranda, Rhiannon E. Lee, Isaline Renard1,2, Shubhanchi Nigam, Gonçalo S. Clemente, Thomas D'Huys, Torsten Ruest, Juozas Domarkas, James A.Thompson, Timothy J. Hubin, Dominique Schols, Christopher J. Cawthorne, Stephen J.Archibald. Copper-64 PET imaging of the CXCR4 chemokine receptor using a cross-bridged cyclam bis-tetraazamacrocyclic antagonist. J Nucl Med. 2020; 61(1):123-128. https://doi.org/10.2967/jnumed.118.218008
28. Giuseppe Lo Sasso1, Walter K. Schlage, Stéphanie Boué1, Emilija Veljkovic, Manuel C. Peitsch and Julia Hoeng. The Apoe$^{-/-}$ mouse model: a suitable model to study cardiovascular and respiratory diseases in the context of cigarette smoke exposure and harm reduction. J Transl Med. 2016; 14(1):1-16. https://doi.org/10.1186/s12967-016-0901-1
29. Wei L, Petryk J, Gaudet C, Kamkar M, Gan W, Duan Y, et al. Development of an inflammation imaging tracer, ^{111}In-DOTA-DAPTA, targeting chemokine receptor CCR5 and preliminary evaluation in an ApoE$^{-/-}$ atherosclerosis mouse model. J Nucl Cardiol. 2019; 26(4):1169–1178. https://doi.org/10.1007/s12350-018-1203-1
30. Valarie M. Truax, Huanyu Zhao, Brooke M. Katzman, Anthony R. Prosser, Ana A. Alcaraz, Manohar T. Saindane, Randy B. Howard, Deborah Culver, Richard F. Arrendale, Prahbakar R. Gruddanti, Taylor J. Evers, Michael G. Natchus, James P. Snyder, Dennis C. Liotta and Lawrence J. Wilson. Discovery of Tetrahydroisoquinoline-Based CXCR4 Antagonists. ACS Med. Chem. Lett. 2013; 4:1025–1030. https://doi.org/10.1021/ml400183q
31. Oliver Demmer, Ingrid Dijkgraaf, Udo Schumacher, Luciana Marinelli, Sandro Cosconati, Eleni Gourni, Hans-Jürgen Wester, Horst Kessler. Design, synthesis, and functionalization of dimeric peptides targeting chemokine receptor CXCR4. J Med Chem. 2011;10;54(21):7648-7662. https://doi.org/10.1021/jm2009716
32. Poul F, Høilund-Carlsen, Michael Sturek, Abass Alavi, Oke Gerke. Atherosclerosis Imaging with (18) F-sodium fluoride PET: state-of-the-art review. European Journal of Nuclear Medicine and Molecular Imaging. 2020; 47:1538–1551. https://doi.org/10.1007/s00259-019-04603-1
33. Ilze Bota,, Isabelle T.M.N. Daissormontb, Alma Zerneckec, Gijs H.M. van Puijveldea, Birgit Krampd, Saskia C.A. de Jagera, Judith C. Sluimerb, Marco Mancab, Veronica Hériasb, Marijke M. Westraa, Martine Bota, Peter J. van Santbrinka, Theo J.C. van Berkela, Lishan Sue, Mona Skjellandf, Lars

Gullestadg, Johan Kuipera, Bente Halvorsenh, Paul Aukrusth, Rory R. Koenend, Christian Weberd, and Erik A.L. Biessena,b Ilze Bot. CXCR4 blockade induces atherosclerosis by affecting neutrophil function. J Mol Cell Cardiol. 2014; 74: 44–52. https://doi.org/10.1016/j.yjmcc.2014.04.021

34. Li X, Yu W, Wollenweber T, Lu X, Wei Y, Beitzke D, et al. [^{68}Ga]Pentixafor PET/MR imaging of chemokine receptor 4 expression in the human carotid artery. Eur J Nucl Med Mol Imaging. 2019;46(8):1616–1625. https://doi.org/10.1007/s00259-019-04322-7
35. Derlin T, Jonigk D, Bauersachs J, Bengel FM. Molecular imaging of Chemokine receptor CXCR4 in non-small cell lung cancer using ^{68}Ga-Pentixafor PET/CT: comparison with ^{18}F-FDG. Clin Nucl Med. 2016; 41:e204–205. https://doi.org/10.1097/RLU.0000000000001092
36. Eric J. Miller, Edgars Jecs, Valarie M. Truax, Brooke M. Katzman, Yesim A. Tahirovic, Robert J. Wilson, Katie M. Kuo, Michelle B. Kim, Huy H. Nguyen, Manohar T. Saindane, Huanyu Zhao, Tao Wang, Chi S. Sum, Mary E. Cvijic, Gretchen M. Schroeder, Lawrence J. Wilson, and Dennis C. Liotta. Discovery of Tetrahydroisoquinoline-Containing CXCR4 Antagonists with Improved in Vitro ADMET Properties. J. Med. Chem. 2018; 61:946–979. https://doi.org/10.1021/acs.jmedchem.7b01420
37. M. Ouimet, T. J. Barrett, and E. A. Fisher, “HDL and reverse cholesterol transport,”Circ. Res. 2019;124(10): 1505–1518. https://doi.org/10.1161/CIRCRESAHA.119.312617
38. Gyu Seong Heo, Deborah Sultan, Yongjian Liu. Current and Novel Radiopharmaceuticals for Imaging Cardiovascular Inflammation. J Nucl Med Mol Imaging. 2020; 64(1): 4–20. https://doi.org/10.23736/S1824-4785.20.03230-6

Figures

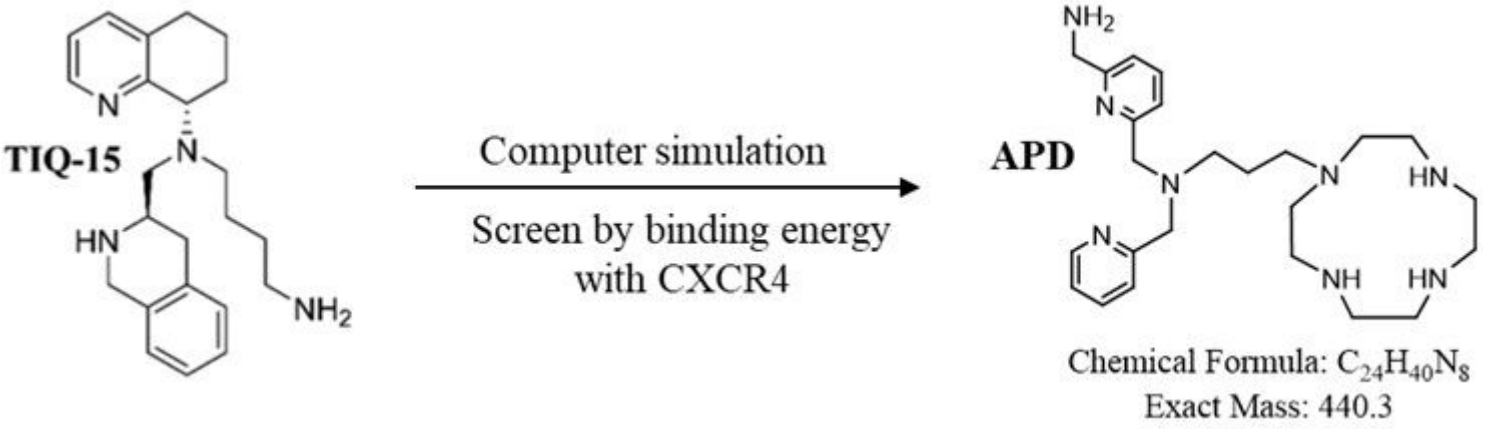

Figure 1

The structure of APD was designed from TIQ-15 by computer simulation and screen by binding energy with CXCR4

Figure 2

Radiochemical purity of [^{68}Ga]-APD was determined by HPLC(up) and TLC(down). HPLC and TLC could separate the impurity and prove the radiochemical purity>90%.

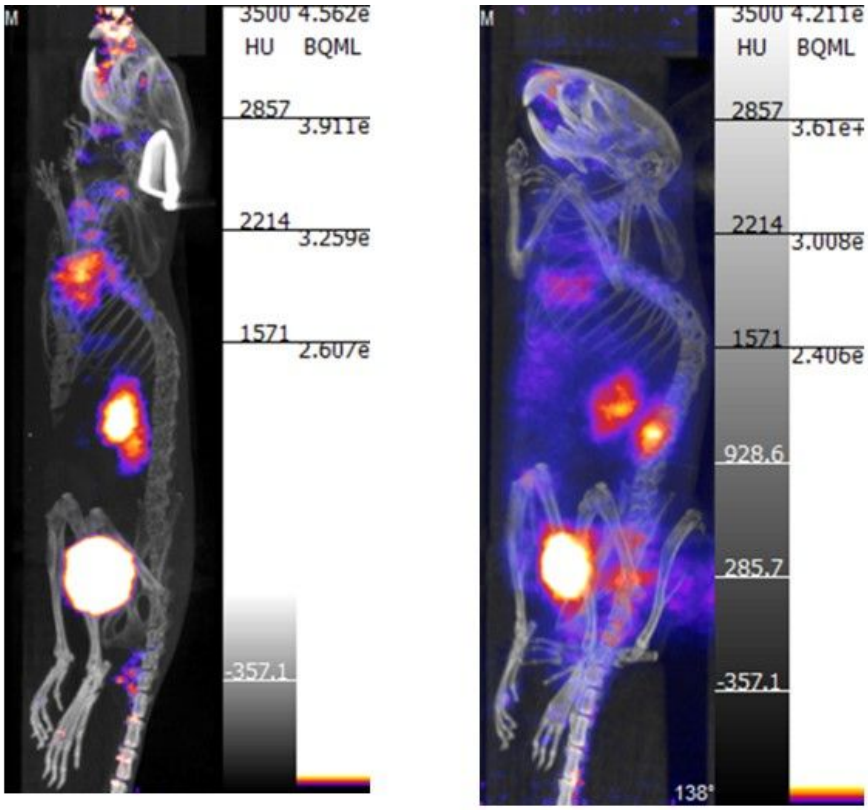

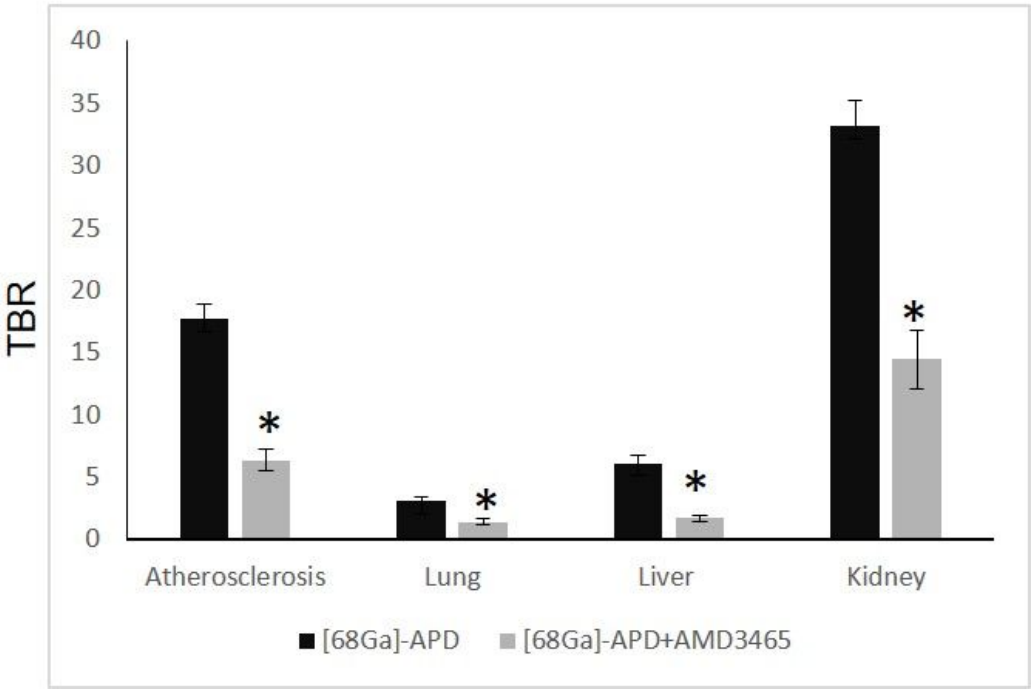

Figure 3

Biodistribution of [^{68}Ga]-APD on a high-fat diet for 12 weeks. [^{68}Ga]-APD was excreted quickly from the kidney and the TBR of atherosclerotic site was 17.68 ± 0.71 after i.v. injection for 0.5 h. CXCR4 antagonist

AMD3465 could inhibit the uptake on the CXCR4-atherosclerotic site, lung, liver and kidney ($P<0.05$).

Figure 4

TBR of [^{68}Ga]-APD on ApoE$^{-/-}$ mice for a high-fat diet 2, 8 and 12 weeks. The TBR was increasing with high-fat diet time.(n=3)

Figure 5

TBR of [^{68}Ga]-APD and [^{68}Ga]-Pentixafor on ApoE$^{-/-}$ mice for a high-fat diet for 12 weeks. The TBR of [^{68}Ga]-APD was 2.06 ± 0.67 at 0.5 h after injection and decreased with time. However, the TBR of [^{68}Ga]-APD was about 8 times higher than [^{68}Ga]-Pentixafor ($P<0.05$).

Figure 6

TBR of [^{68}Ga]-APD, [^{18}F]-FDG and [^{18}F]-NaF on ApoE$^{-/-}$mice high fat diet for 10 weeks. [^{18}F]-FDG was major distributed in the myocardium. [^{68}Ga]-APD distributed specifically in the atherosclerotic site. [^{18}F]-NaF could not find to target on heart and atherosclerotic site.

Figure 7

Tissue slide autoradiogram of [^{68}Ga]-APD had shown obvious high radioactivity accumulating in the aorta region but not on the heart.